Conditional knockout of *Cdc20* attenuates osteogenesis in craniofacial bones

Yawen Cheng [1], Yangge Du [1], Xiao Zhang, Ping Zhang [*], Yunsong Liu [*]

Department of Prosthodontics, Peking University School and Hospital of Stomatology, National Engineering Laboratory for Digital and Material Technology of Stomatology, National Clinical Research Center for Oral Diseases, Beijing Key Laboratory of Digital Stomatology, Beijing, China

ARTICLE INFO

ABSTRACT

Craniofacial bone defects cause significant problems to patients with harmful consequences. Mesenchymal stem cells (MSCs) can self-renew and exhibit multilineage differentiation, which could be applied to bone regeneration. However, craniofacial bone tissue MSCs have unique properties, differing in their characteristics to MSCs derived from long bones. CDC20 promotes osteogenic differentiation in long bones; however, its role in craniofacial bone tissues remains unknown. In this study, we found that *Cdc20* conditional knockout in mice triggered distinctive cranial and mandibular bone loss. Moreover, the osteogenic differentiation potential of cranial suture-derived MSCs and mandibular bone marrow-derived MSCs was impaired in *Cdc20* conditional knockout mice. The conditional knockout of *Cdc20* impaired osteogenesis in craniofacial bones. Our findings provide new insights into craniofacial bone regeneration and the treatments of craniofacial bone-related diseases.

1. Introduction

Bone defects are common clinical conditions with severe detrimental effects on the bodily functions and quality of life of patients. Craniofacial bone abnormalities can arise due to tumors, traumas, congenital diseases, or infections, and severely jeopardize mastication, pronunciation, and facial esthetics. Therefore, they cause a considerable medical burden on individuals and society, and advanced treatment strategies for craniofacial bone loss are urgently needed (Fliefel et al., 2017). Craniofacial bone regeneration is a promising and rapidly evolving field. Recent advances in molecular and cell biology enable the development of treatments targeting genes in craniofacial stem cells, providing a novel approach to restoring craniofacial bone tissue.

Cell division cycle protein 20 (CDC20) is an important cell-cycle regulator involved in mitosis. CDC20 activates and binds to anaphase-promoting complex/cyclosome (APC/C), which enables the ubiquitination and degradation of substrates. Therefore, CDC20 serves as an integrator of intracellular signaling cascades, regulating progression

through mitosis (Yu, 2007). Besides regulating the cell cycle, CDC20 is involved in the regulation of other processes such as apoptosis (Harley et al., 2010), human malignancies (Chang et al., 2012), neuronal connectivity, and brain plasticity (Yang et al., 2009). CDC20 also plays an essential role in osteogenesis in long bones by promoting the ubiquitination and degradation of p65 (Du et al., 2021). However, whether CDC20 exerts unique effects on craniofacial bone tissue remains unknown.

Craniofacial bone tissue stem cells comprise mandibular bone marrow-derived mesenchymal stem cells (MSCs) and cranial bone-derived MSCs. Mandibular bone marrow-derived MSCs play a significant role in mandibular bone remodeling and healing (Chung et al., 2009; Lee et al., 2019). Cranial sutures serve as the osteogenic front for intramembranous ossification, and the major population of cranial bone-derived MSCs is derived from cranial sutures (Zhao and Chai, 2015; Li et al., 2021). Both types of MSCs possess the ability to differentiate into osteoprogenitors and to further give rise to osteoblasts (Kaltschmidt et al., 2012). *Sp7-Cre* mice enable targeted gene deletion in

Table 1

Sequences of genotyping primers.

Name	Primer sequence (5′–3′)	
Cdc20 5′loxP-F	CCTAAACTATGTGGAGTTCAAGGCCA	WT:202 bp
Cdc20 5′loxP-R	AGGATCTAGGATCTAGGTGACTCCC	Mut:321 bp
Cdc20 3′loxP-F	GAAGCAGCTCCTGTCTTGGAGTTGT	WT:405 bp
Cdc20 3′loxP-R	CCACAGCCTGGGTGGAATGGATAAA	Mut:490 bp
Sp7-Cre WT-F	TACCAGAAGCGACCACTTGAGC	263 bp
Sp7-Cre WT-R	CGCCAAGAGAGCCTGGCAAG	263 bp
Sp7-Cre Mut-F	TACCAGAAGCGACCACTTGAGC	445 bp
Sp7-Cre Mut-R	GCACACAGACAGGAGCATCTTC	445 bp

osteoprogenitors and are used to generate mouse models for investigating the roles of specific genes in bone development (Liu et al., 2017; Chen et al., 2021). Craniofacial bone-derived MSCs differ from long bone marrow-derived MSCs in terms of developmental origin, clinical performance, proliferation, and differentiation potency (Helms and Schneider, 2003; Yamaza et al., 2011; Lloyd et al., 2017), suggesting that there is a discrepancy between craniofacial and long bone regeneration. Thus, it is essential to investigate whether CDC20 plays a unique role in mandibular and cranial bone regeneration.

In this study, we characterized the function of *Cdc20* in the regulation of craniofacial bone formation. *Cdc20* contributed to craniofacial bone regeneration, revealing its potential role as a target for improving therapeutic strategies to treat craniofacial bone-related diseases.

2. Materials and methods

2.1. Generation and genotyping of mouse models

Cdc20$^{f/f}$ and *Sp7-Cre;Cdc20$^{f/f}$* mice were generated as previously described (Du et al., 2021). In brief, Cdc20-floxed (*Cdc20$^{f/+}$*) mice were generated using a clustered regularly interspaced short palindromic repeats (CRISPR)/Cas9-based extreme genome editing (EGE) system (Biocytogen Co., Ltd., Beijing, China). The targeting vector, single guide RNAs (sgRNAs), and Cas9 mRNA were co-injected into C57BL/6 N mouse zygotes. The targeting vector was synthesized in vitro and contained genomic DNA spanning exons 1–7 of the mouse *Cdc20* gene flanked by two loxP sites. Homology arms were also incorporated at the 5′ and 3′ regions. Using the CRISPR design tool (http://www.sanger.ac. uk/htgt/wge/) and the UCA™ CRISPR efficiency evaluation kit (Biocytogen Co., Ltd.), two sgRNAs were generated to target the upstream region of exon 1 and the downstream region of exon 7 of *Cdc20*. After injection, the surviving two-cell stage zygotes were transplanted into KM albino pseudo-pregnant females to generate founder mice bearing the floxed *Cdc20* allele. Verification of the mouse genotypes was carried out by PCR amplification, DNA sequencing, and Southern blot analysis.

Sp7-Cre mice were obtained from Biocytogen Co., Ltd. An F2A-iCre sequence cassette was placed between the coding sequence of exon 2 and the 3′ untranslated region of the *Sp7* gene in C57BL/6 ES cells. For detailed information on the iB-Sp7-iCre mice, review https://biocyt

ogen.com/products/cre-mouse-rat-models/b-sp7-osx-icre-mice/. *Sp7-Cre* mice were then bred with *Cdc20$^{f/f}$* mice to generate iCre-positive, loxp-homozygous (*Sp7-Cre;Cdc20$^{f/f}$*) conditional knockout mice and their corresponding littermates. Genotyping primers are shown in Table 1.

Sp7-Cre;Cdc20$^{f/f}$ mice were used as the experimental group, whereas *Cdc20$^{f/f}$* were used as the control group. A single mouse was used as the experimental unit, and each group contained three mice. All healthy *Sp7-Cre;Cdc20$^{f/f}$* and *Cdc20$^{f/f}$* mice was included. All animal procedures and experiments were carried out according to the guidelines of the Institutional Animal Care and Use Committee of the Peking University Health Science Center (LA2014233).

2.2. Harvesting and culturing of primary cells

Proliferation medium (PM) contained α-minimum essential medium (Invitrogen, Carlsbad, CA, USA), 10% fetal bovine serum (PAA Laboratories GmbH, Linz, Austria), and 1% penicillin/streptomycin (Invitrogen). Osteogenic medium (OM) comprised standard PM and 10 mM β-glycerophosphate, 0.2 mM ascorbic acid, and 100 nM dexamethasone.

Primary mouse cranial suture-derived MSCs were obtained from 4-day-old mice as described previously (Xu et al., 2007; James et al., 2008). Sagittal sutures on cranial bones with 0.5-mm bony margins on either side were harvested to minimize tissue heterogeneity. Then, the underlying dura mater and the overlying pericranium were dissected from the suture mesenchyme, and the remaining suture tissue was minced into tiny blocks to expose the suture mesenchyme and explanted into culture dishes (Corning, Corning, NY, USA) containing PM. After 2 days, cranial suture-derived MSCs migrated from the explant tissue blocks and were observed by microscope.

The separation procedures of primary mouse mandibular bone marrow-derived MSCs were performed as previously described (Yamaza et al., 2011). First, 6-week-old mice were sacrificed, mandibles were excised, and incisors and molars were removed. Subsequently, the bones were cut up, and all nucleated cells from the mandibular bones were isolated by digestion with collagenase type 2 and type 4 (15 mg/mL; Worthington Biochemical Corporation, Lakewood, NJ, USA) for 1 h at 37 °C. The dissociated cells were filtered through a 40-mm strainer, and the supernatants were collected and seeded into culture dishes containing PM. Cells were maintained at 37 °C with 5% CO_2. The medium was replenished after 2 days to remove non-adherent cells. Cells passaged less than two times were used for all experiments. For osteogenic differentiation, two types of cells were seeded in 12-well plates and induced in PM and OM for 7 days for further experiments.

2.3. Cell counting kit-8 assay

For cell proliferation assays, cells were seeded in 96-well plates and cultured at 2×10^3 cells per well in PM. At day 0, 1, 3, 5, 7, the cell number was evaluated with a Cell Counting Kit-8 (CCK8, Dojindo Laboratories, Kumamoto, Japan) according to the manufacturer's instructions. Optical density (OD) at 450 nm was measured using a microplate reader (ELX808, BioTek) and growth curves were drawn according to the OD values (n = 3).

2.4. RNA isolation and quantitative real-time polymerase chain reaction (qRT-PCR)

Total RNA was extracted with TRIzol reagent (Invitrogen) from cells cultured in PM or OM for 7 days, and a NanoDrop 8000 spectrophotometer (Pierce Thermo Scientific, Waltham, MA, USA) was used to measure the purity and concentration of the total RNA. Reverse transcription was performed with a PrimeScript RT Reagent Kit (#RR037A; Takara, Tokyo, Japan). qRT-PCR was performed using a 7500 Real-Time PCR Detection System (Applied Biosystems, Foster City, CA, USA) and SYBR Green Master Mix (Roche Applied Science, Mannheim, Germany).

Table 2

Sequences of PCR primers.

Name	Sense strand (5′–3′)	Antisense strand (5′–3′)
Gapdh	CAGGAGAGTGTTTCCTCGTCC	TGAAGGGGTCGTTGATGGCA
Cdc20	CTCAAAGGACACACAGCACGG	CGCCACAACCGTAGAGTCTCA
Alp	TGACCTTCTCTCCTCCATCC	CTTCCTGGGAGTCTCATCCT
Runx2	CCGGGAATGATGAGAACTA	ACCGTCCACTGTCACTTT

a

exon1-7   Cdc20

▶ : loxP

✂ : Cre recombinase

Sp7-Cre   ×   *Cdc20^{f/f}*   →   *Sp7-Cre;Cdc20^{f/f}*

b

Cdc20^{f/f}   *Sp7-cre;Cdc20^{f/f}*

Sp7-Cre   Mut (445bp)

Sp7-Cre   WT (263bp)

Cdc20   Mut (321bp)

Fig. 1. Construction and genotyping of the *Cdc20* conditional knockout mouse model. (a) Schematic diagram depicting the *Cdc20* gene knockout strategy and the construction process of *Cdc20* conditional knockout mice. (b) Representative images of DNA electrophoresis gels depicting the genotypes of the indicated mice. (c, d) Relative *Cdc20* mRNA expression levels in primary cells derived from mandibular bone (c) and cranial bone (d) in *Sp7-Cre;Cdc20^{f/f}* mice and their littermate control mice.

c

Cdc20 mRNA in mandibular bone (fold)

Cdc20^{f/f}   *Sp7-Cre;Cdc20^{f/f}*   ***

d

Cdc20 mRNA in cranial bone (fold)

Cdc20^{f/f}   *Sp7-Cre;Cdc20^{f/f}*   ***

Gene expression levels were calculated using the $^{\Delta\Delta}$CT method and normalized to glyceraldehyde-3-phosphate dehydrogenase. The primer sequences used are listed in Table 2.

2.5. Alkaline phosphatase (ALP) staining and quantification

Primary mouse cranial suture-derived MSCs and mandibular bone marrow-derived MSCs were seeded in 12-well plates. After 7 days of culture in PM or OM, the cells were washed with phosphate-buffered saline (PBS), fixed in 95% cold ethanol for 30 min, and then washed again with PBS. ALP staining was performed using a nitroblue tetrazolium/5-bromo-4-chloro-3-indolyl phosphate staining kit (CoWin Biotech, Jiangsu, China) according to the manufacturer's instructions. The cells were then gently rinsed with distilled water, and images were taken.

To quantify ALP activity, cells were washed with PBS and lysed with 1% Triton X-100 on ice, and centrifuged at 13,362×*g* for 30 min at 4 °C. A BCA protein assay kit (Pierce Thermo Scientific) was used to measure the total protein concentration for normalization. ALP activity was quantified using an ALP assay kit (Nanjing Jiancheng Bioengineering Institute, Jiangsu, China). The ALP activity was calculated according to the absorbance at 520 nm.

2.6. Micro-computed tomography (micro-CT) and soft X-ray

To evaluate differences in bone mass and microarchitecture in *Cdc20^{f/f}* and *Sp7-Cre;Cdc20^{f/f}* mice, cranial bones and mandibular bones were scanned using an Inveon MM system (Siemens, Munich, Germany) after fixation in 4% paraformaldehyde for 2 days. Images were acquired at a pixel size of 8.82 μm, current of 220 μA, voltage of 60 kV, and exposure time of 1500 ms. Bone morphometric parameters including

bone volume/total volume (BV/TV), trabecular number (Tb.N), trabecular spacing(Tb. Sp), and bone mineral density (BMD) in the region of interest (ROI) were calculated using an Inveon Research Workplace (Siemens). The examiners blinded to the treatment group when they conducted their analysis.

Soft X-ray images were taken after fixation in 4% paraformaldehyde for 2 days using a Senographe Essential Version ADS_55.20 instrument (GE Medical Systems, Little Chalfont, England) at 22 mA current and 25 kV voltage. The gray value was calculated using ImageJ software. The examiners blinded to the treatment group when they conducted their analysis.

2.7. Histology and hematoxylin and eosin (H&E) staining

After fixing in 4% paraformaldehyde for 2 days, the cranial and mandibular bone specimens were soaked in 0.5 M ethylenediaminetetraacetic acid at 37 °C for 3 weeks for decalcification. The decalcifying fluid was changed every 2 days. Afterwards, bone tissues were embedded in paraffin, cut into 5-μm tissue sections, and subjected to deparaffinization and rehydration. Sections were stained with H&E for histological observation.

2.8. Statistical analyses

Means and standard deviations presented in text and figures were calculated using at least three experiments per group. Statistical analyses were performed using GraphPad software (GraphPad Software, Inc., La Jolla, CA, USA). In the figures, bar graphs represent means, and error bars represent the standard deviation. Independent two-tailed Student's *t*-tests were used to evaluate the differences between two groups, and one-way analysis of variance followed by Tukey's post hoc
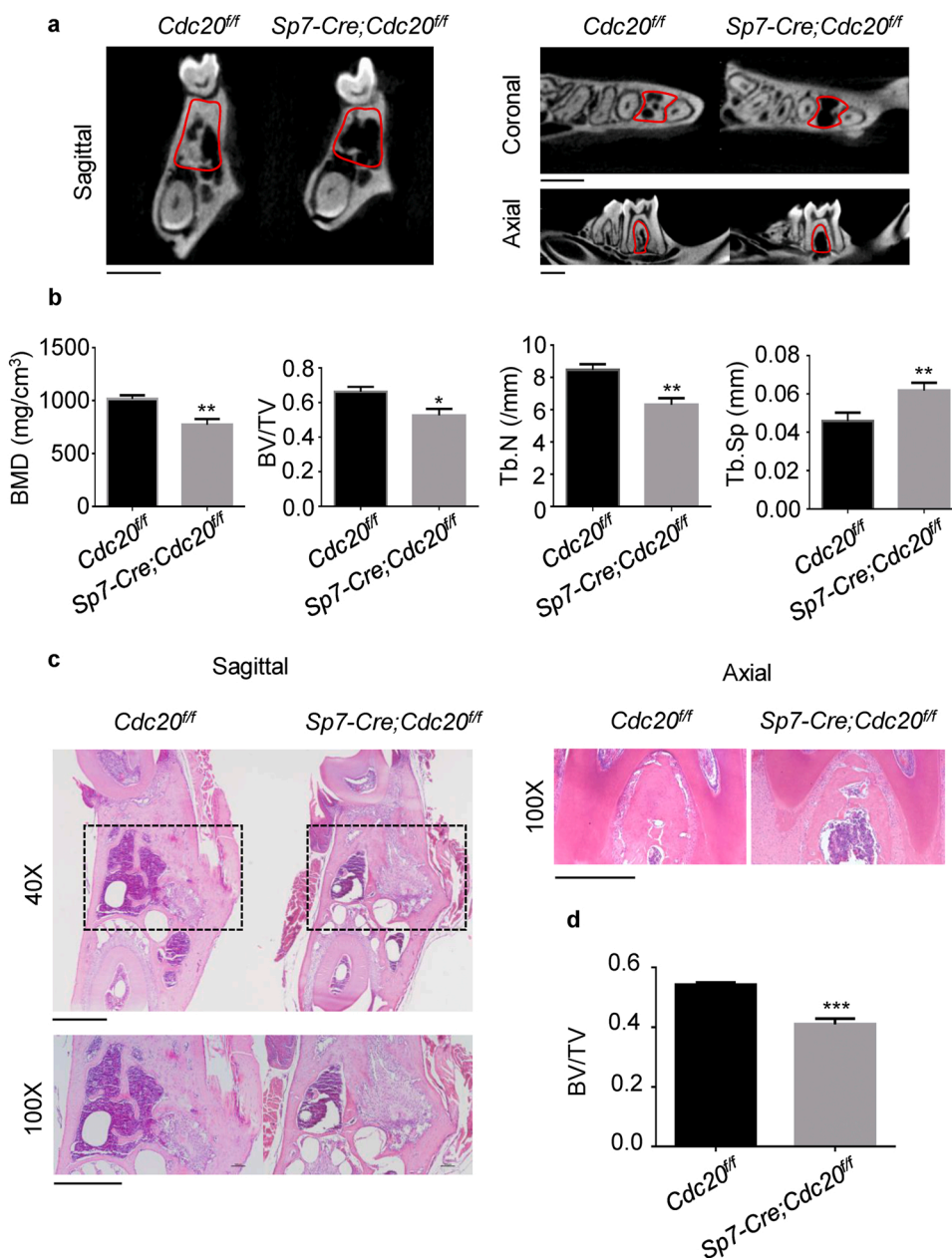
Fig. 2. Conditional knockout of *Cdc20* impaired osteogenesis in mandibular bone. (a) Representative micro-computed tomography images of the mandibular bones of 6-week-old *Sp7-Cre;Cdc20^{f/f}* mice and their control littermates. The red borders show the ranges of the regions of interest (ROIs) examined for the histomorphometric analyses (range of furcation to apex of the first molars). Scale bar, 1.0 mm. (b) Histomorphometric analyses of ROIs in mandibular bones of 6-week-old *Cdc20^{f/f}* and *Sp7-Cre;Cdc20^{f/f}* mice. (c) Representative hematoxylin and eosin staining of mandibular bones from *Sp7-Cre;Cdc20^{f/f}* and their littermate control mice. The lower panels show the magnified images of the area indicated by a black dotted line. Scale bar, 500 μm. (d) Histologic quantitative analyses of bone volume/total volume (BV/TV) of mandibular bones from 6-week-old *Cdc20^{f/f}* and *Sp7-Cre;Cdc20^{f/f}* mice. Results are presented as the mean ± standard deviation (n = 3). Statistical analyses were performed using a two-sided unpaired Student's *t*-test. (*$p < 0.05$; **$p < 0.01$; ***$p < 0.001$).

tests were performed for comparisons between more than two groups. A two-tailed value of $p < 0.05$ was considered to represent statistical significance.

3. Results

3.1. Construction and genotyping of the Cdc20 conditional knockout mouse model

We generated a *Cdc20* conditional knockout mouse model using the Cre/loxP system to investigate the role of *Cdc20* in craniofacial bone in vivo. The *Cdc20^{f/f}* and *Sp7-Cre;Cdc20^{f/f}* mouse models were developed as previously described (Du et al., 2021). In brief, *Cdc20*-floxed (*Cdc20^{f/+}*) mice were generated using a CRISPR/Cas9-based EGE system. Then, we crossed *Cdc20^{f/+}* with *Sp7-Cre* mice to generate the *Sp7-Cre;Cdc20^{f/f}* model. In *Sp7-Cre;Cdc20^{f/f}* mice, cre recombinase-mediated removal of the exon 1–7 led to the translation termination of *Cdc20* (Fig. 1a). Genotyping was carried out by PCR

amplification using mice tail extracts and DNA gel electrophoresis (Fig. 1b). *Sp7-Cre;Cdc20^{f/f}* mice were used as the experimental group, whereas *Cdc20^{f/f}* were used as the control group. We performed qRT-PCR to examine the efficiency of the *Cdc20* conditional knockout mouse model; *Cdc20* mRNA expression levels were relatively low in primary cells derived from mandibular and cranial bone (Fig. 1c,d). These results showed that we successfully constructed *Cdc20* conditional knockout mice and that *Cdc20* expression was suppressed in cranial and mandibular bones.

3.2. Conditional Cdc20 knockout impaired osteogenesis in mandibular bone

Micro-CT and H&E staining analyses revealed that the mandibular bone microarchitecture of 6-week-old *Sp7-Cre;Cdc20^{f/f}* mice exhibited significant deterioration. The BMD and BV/TV parameters of mandibular bones were significantly lower in 6-week-old *Sp7-Cre;Cdc20^{f/f}* mice compared to in their *Cdc20^{f/f}* littermates. The Tb.N was lower and Tb.Sp
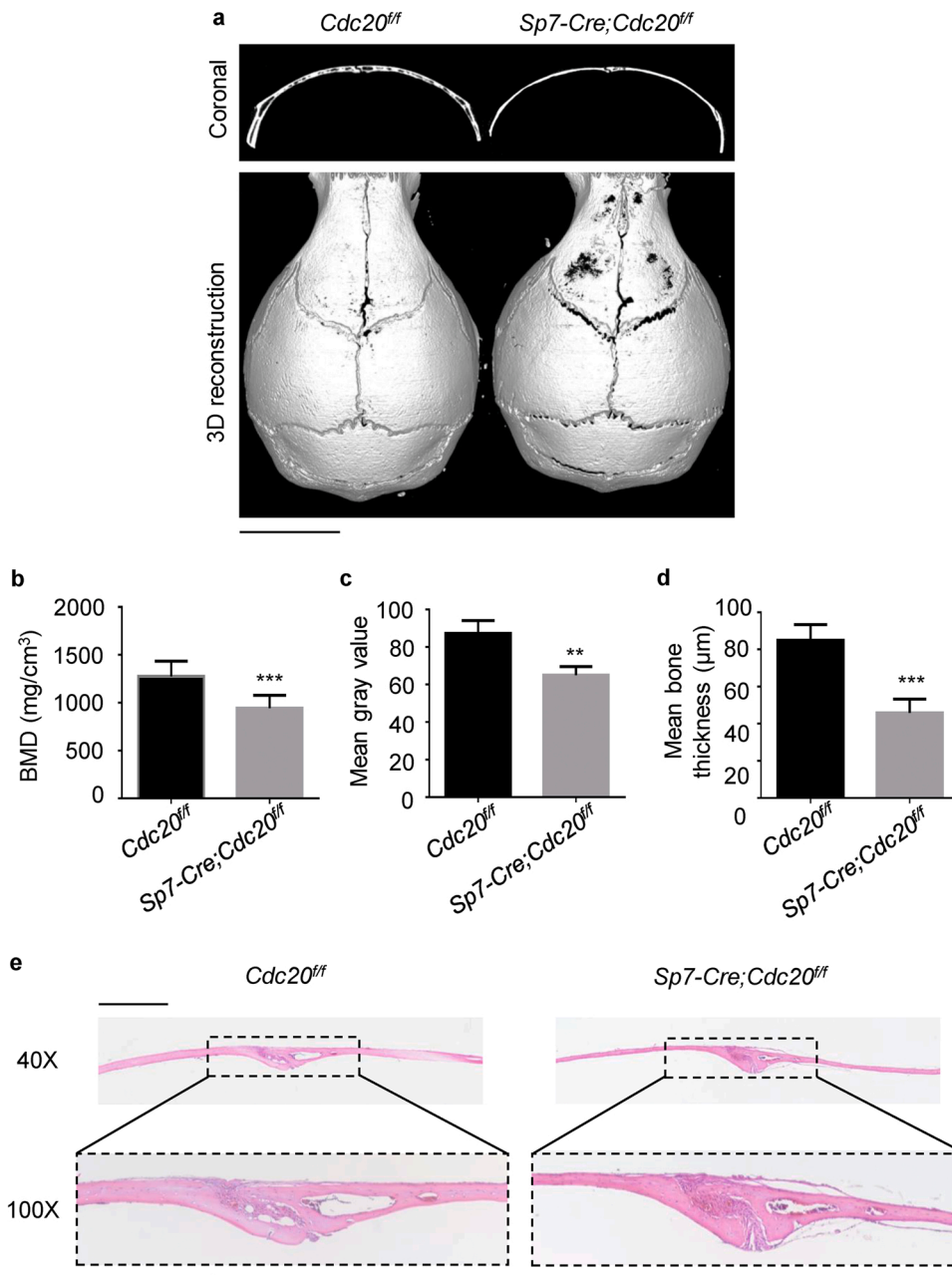
Fig. 3. Conditional knockout of *Cdc20* reduced osteogenesis in cranial bone. (a) Representative micro-computed tomography images of cranial bones of 6-week-old *Sp7-Cre;Cdc20^f/f* mice and their littermate control mice. Scale bar, 5.0 mm. (b) Bone mineral density measurement of cranial bones taken from 6-week-old *Cdc20^f/f* and *Sp7-Cre;Cdc20^f/f* mice. (c) Quantitative X-ray analysis of cranial bones from 6-week-old *Cdc20^f/f* and *Sp7-Cre;Cdc20^f/f* mice. (d) Histologic measurements of cranial bone thickness of 6-week-old *Cdc20^f/f* and *Sp7-Cre;Cdc20^f/f* mice. (e) Representative hematoxylin and eosin staining images of cranial bone from *Sp7-Cre; Cdc20^f/f* mice and littermate control mice. The left panels show the magnified images of the area indicated by a black dotted line. Scale bar, 500 μm. Results are presented as the mean ± standard deviation (n = 3). Statistical analyses were performed using two-sided unpaired Student's *t*-tests (**$p < 0.01$; ***$p < 0.001$).

was higher in 6-week-old *Sp7-Cre;Cdc20^f/f* mice compared to in the control mice (Fig. 2a,b). H&E staining and quantitative BV/TV analysis on histological sections revealed mandibular bone impairments in 6-week-old *Sp7-Cre;Cdc20^f/f* mice compared with their littermates (Fig. 2c,d). Our results suggest that downregulating *Cdc20* expression impaired bone formation in the mandible.

3.3. Conditional knockout of Cdc20 reduced osteogenesis in cranial bone

Micro-CT and soft X-ray scans revealed that massive bone loss occurred in the cranial bones of 6-week-old *Sp7-Cre;Cdc20^f/f* mice. The coronal and three-dimensional (3D) reconstruction views displayed a distinct reduction in cranial bone thickness in *Sp7-Cre;Cdc20^f/f* mice (Fig. 3a). The BMD parameter of cranial bones was significantly lower in 6-week-old *Sp7-Cre;Cdc20^f/f* mice compared with their *Cdc20^f/f* littermates (Fig. 3b). Similarly, the gray values calculated from soft X-ray scans were lower in the experimental group compared to the control

group, suggesting that the BMD was reduced in the *Sp7-Cre;Cdc20^f/f* mice (Fig. 3c). H&E staining and quantitative cranial bone thickness measurements revealed that the bone mass was lower in the cranial bones of 6-week-old *Sp7-Cre;Cdc20^f/f* mice compared with their littermates (Fig. 3d,e). These results suggest that downregulating *Cdc20* suppressed osteogenesis in cranial bone.

3.4. Loss of Cdc20 attenuated the osteogenic differentiation of mandibular bone marrow-derived MSCs

To further explore the effect of CDC20 on mandibular bone marrow-derived MSCs, we obtained primary cells through collagenase dissociation. We carried out qRT-PCR, showing that *Cdc20* mRNA expression levels in mandibular bone marrow-derived MSCs were relatively low in the experimental group compared with the control group (Fig. 4a). The Cell counting kit-8 assay revealed that there was no distinctive difference of cell proliferation rate in mandibular bone marrow-derived MSCs

mandibular bone marrow-derived MSCs

a

b

c

d

e

f
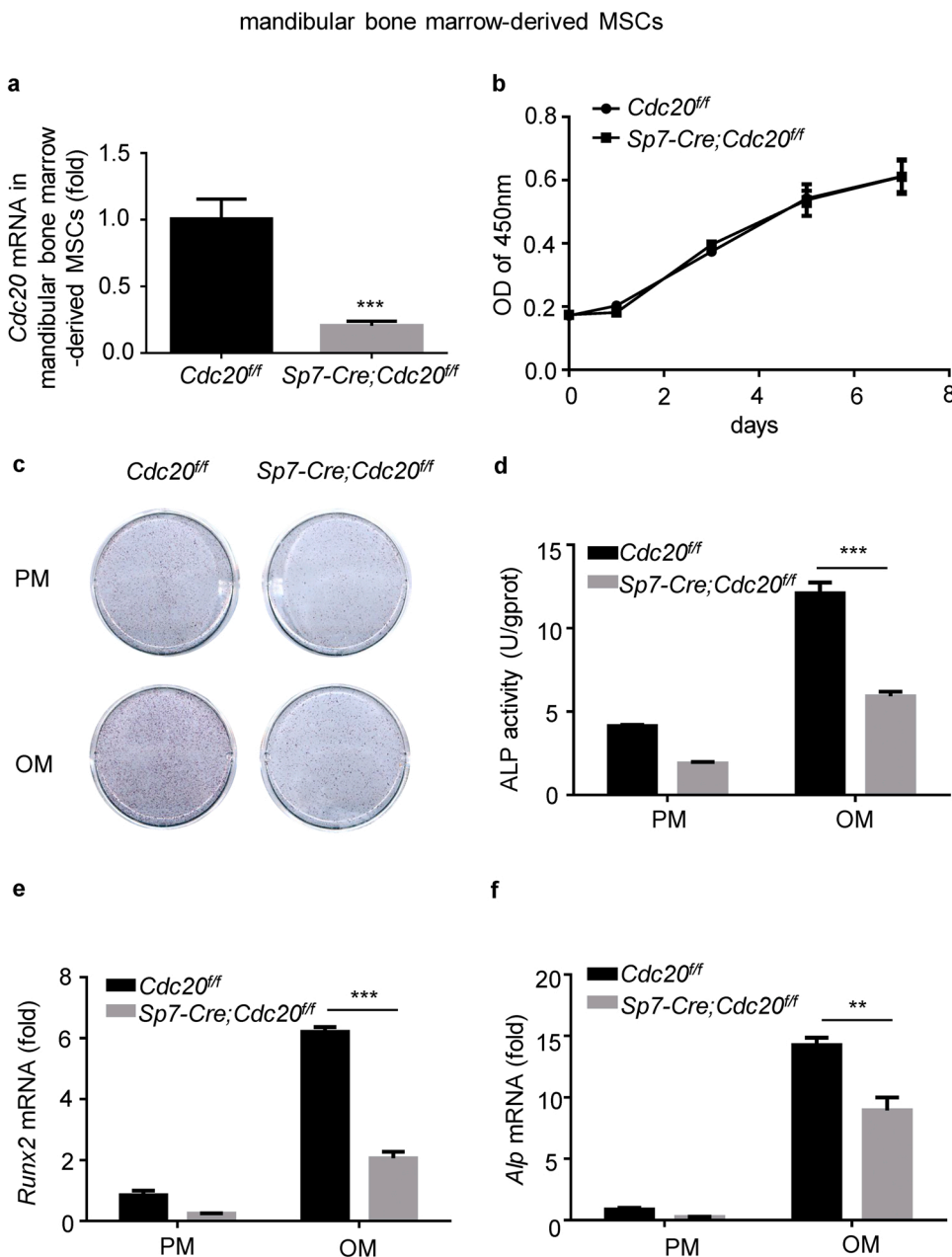
Fig. 4. *Cdc20* silencing attenuated osteogenic differentiation of mandibular bone marrow-derived mesenchymal stem cells (MSCs). (a) Relative *Cdc20* mRNA expression levels in mandibular bone marrow-derived MSCs in *Sp7-Cre;Cdc20^{f/f}* mice and their littermate control mice. (b) Cell counting kit-8 assay of mandibular bone marrow-derived MSCs from *Sp7-Cre; Cdc20^{f/f}* and *Cdc20^{f/f}* mice at day 0, 1, 3, 5, 7. (c, d) Alkaline phosphatase (ALP) staining (c) and ALP activity (d) of mandibular bone marrow-derived MSCs harvested from *Sp7-Cre; Cdc20^{f/f}* and *Cdc20^{f/f}* mice after osteogenic induction for 7 days. (e, f) The relative mRNA expression levels of the osteogenic markers *Runx2* (e) and *Alp* (f) in mandibular bone marrow-derived MSCs were determined by quantitative real-time polymerase chain reaction after 7 days of culturing in proliferation medium or osteogenic medium. Results are presented as the mean ± standard deviation (n = 3). Statistical analyses were performed using a one-way analysis of variance and a post hoc test (**$p < 0.01$; ***$p < 0.001$).

from *Sp7-Cre;Cdc20^{f/f}* mice and their *Cdc20^{f/f}* littermates (Fig. 4b). ALP staining (Fig. 4c) and ALP activity quantification (Fig. 4d) of the primary cells indicated that CDC20 silencing in mandibular bone marrow-derived MSCs inhibited their osteogenic differentiation. The relative mRNA expression levels of the osteogenic differentiation markers *Runx2* and *Alp* revealed that osteogenic differentiation was downregulated in the mandibular bone marrow-derived MSCs of *Sp7-Cre;Cdc20^{f/f}* mice compared with those of their *Cdc20^{f/f}* littermates after 7 days of osteogenic culture (Fig. 4e,f). Our results suggested that the *Cdc20* knockdown reduced the osteogenic differentiation potential without affecting the proliferation of mandibular bone marrow-derived MSCs.

3.5. Cdc20 silencing inhibited osteogenic differentiation of cranial suture-derived MSCs

Primary cranial suture-derived MSCs were separated from cranial bone tissue to evaluate the impact of *Cdc20* silencing. qRT-PCR results revealed that *Cdc20* mRNA expression level is successfully

downregulated (Fig. 5a). Determined by CCK8 assay, cell proliferation of cranial suture-derived MSCs from *Sp7-Cre;Cdc20^{f/f}* mice and their *Cdc20^{f/f}* littermates didn't show a significant difference (Fig. 5b). The primary cranial suture-derived MSCs were subjected to ALP staining (Fig. 5c) and ALP activity quantification (Fig. 5d) after 7 days of osteogenic induction, which revealed that *Cdc20* silencing reduced the osteogenic differentiation potential of cranial suture-derived MSCs. Furthermore, the relative *Runx2* and *Alp* mRNA expression levels were lower in the experimental group compared to in the control group (Fig. 5e,f). These results suggest that, similar to mandibular bone marrow-derived MSCs, *Cdc20* downregulation impairs osteogenic differentiation in cranial suture-derived MSCs.

4. Discussion

During cell division, CDC20 plays a key role in the formation of the checkpoint complex, which prevents mitotic exit and regulates the biochemical functions of several proteins (Lara-Gonzalez et al., 2021).

Cranial suture-derived MSCs

a

b

c

d

e

f
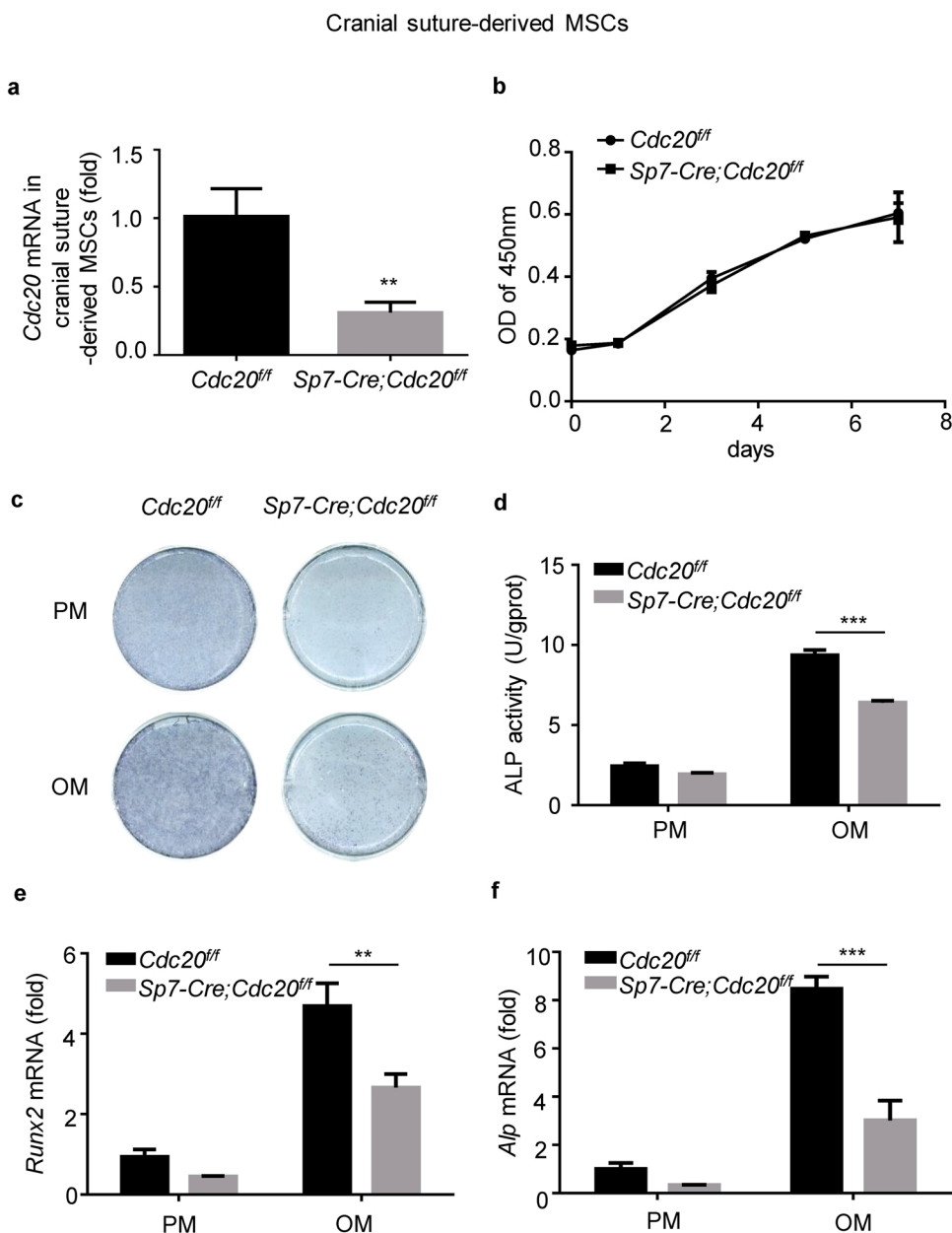
Fig. 5. Loss of *Cdc20* inhibited osteogenic differentiation of cranial suture-derived mesenchymal stem cells (MSCs). (a) Relative *Cdc20* mRNA expression levels in cranial suture-derived MSCs in *Sp7-Cre;Cdc20^{f/f}* mice and their littermate control mice. (b) Cell counting kit-8 assay of mandibular bone marrow-derived MSCs from *Sp7-Cre;Cdc20^{f/f}* and *Cdc20^{f/f}* mice at day 0, 1, 3, 5, 7. (c, d) Alkaline phosphatase (ALP) staining (c) and ALP activity (d) of cranial suture-derived MSCs harvested from *Sp7-Cre;Cdc20^{f/f}* and *Cdc20^{f/f}* mice after osteogenic induction for 7 days. (e, f) The relative mRNA expression levels of the osteogenic markers *Runx2* (e) and *Alp* (f) in cranial bone marrow-derived MSCs were examined by quantitative real-time polymerase chain reaction after 7 days of culturing in proliferation medium or osteogenic medium. Results are presented as the mean ± standard deviation (n = 3). Statistical analyses were performed using a one-way analysis of variance and post hoc test (**$p < 0.01$; ***$p < 0.001$).

CDC20 expression is also elevated in high-grade cancers and has been linked to poor prognoses. Furthermore, CDC20 is highly expressed in breast cancer patients, and *Cdc20* overexpression is associated with aggressive breast cancer (Karra et al., 2014). Silencing of CDC20 induces G2/M cell cycle arrest, inhibits cell growth, and retards colony formation in lung cancer cells (Kidokoro et al., 2008). Migration and invasion inhibitor protein interacts with CDC20 and inhibits APC/C-mediated degradation of cyclin B1, which in turn inhibits glioma development and progression (Ji et al., 2010). Therefore, specific CDC20 inhibitors may be a strategy for the treatment of human cancers. However, few studies have reported the relationship between CDC20 and bone formation. Conditionally knocking out CDC20 decreases long bone formation in mice, and reduces the osteogenic differentiation of bone marrow MSCs via p65 degradation (Du et al., 2021). In the present study, we examined the role of CDC20 in cranial and mandibular bone, and the results were consistent with the previous research outlined above.

Sp7 transcription factor 7/Osterix (Sp7/Osx) is a C2H2-type zinc finger transcription factor, which is a putative master regulator of osteoblast lineage progression. Generated by osteoprogenitors, Sp7/Osx is essential for MSCs to differentiate into osteoblasts and is involved in bone formation during postnatal growth (Nakashima et al., 2002; Celil and Campbell, 2005; Zhou et al., 2010). The Cre/loxP system has been widely used to generate conditional gene knockout mice (Rodda and McMahon, 2006). *Sp7-Cre* mice can be used to specifically target skeletal tissues, including craniofacial bone. For example, autophagy-related genes were knocked down in craniofacial bone using the *Sp7-Cre* strain, leading to compromised craniofacial bone development and indicating the significant role of autophagy in craniofacial bone formation (Thomas et al., 2019). *Fgfr3* was specifically activated by knocking out the NEO sequence in osteoprogenitors, which showed that *Fgfr3* impairs craniofacial bone growth (Biosse Duplan et al., 2021). The targeted deletion of Dicer in cranial osteoblast precursor cells using the *Sp7-Cre* system rescued suture defects and increased cranial bone mass (Atsawasuwan et al., 2017). By contrast, osteoblast-specific Irx3 knockout mice (Irx3^{fl/fl}/Osx-Cre^+ mice) exhibited decreased cranial bone mineralization (Cain et al., 2016). Reduced IFT140 expression specifically in Osx-positive cells delayed healing processes in alveolar

bone sockets and reduced differentiation and proliferative potency in alveolar bone marrow-derived MSCs (Zhou et al., 2021). Osteoblastic cell lineages are required during craniofacial development to regulate bone formation (Percival and Richtsmeier, 2013). In this study, *Sp7*-driven *Cdc20* knockout mice were an effective tool to investigate the role of CDC20 on craniofacial bones.

In this study, we constructed a *Cdc20* conditional knockout mouse model considering that CDC20 is a crucial cell cycle-related factor and systematic knockout of *Cdc20* causes embryonic lethality. Our results revealed that conditional knockout of *Cdc20* in osteoprogenitors via Sp7-Cre remarkably attenuates osteogenesis in craniofacial bones. Interestingly, we found that there is no significant difference in cell proliferation ability of primary mandibular bone marrow-derived MSCs and cranial suture-derived MSCs separated from *Sp7-Cre;Cdc20^{f/f}* mice and *Cdc20^{f/f}* mice. Therefore, the deterioration of bone formation is due to the decreases in osteogenic differentiation, but not proliferation. Zhao et al. (2021) and Gao et al. (2021) reported that downregulation of CDC20 suppressed cell proliferation in hepatocellular carcinoma cells and osteosarcoma cells, respectively. The possibility is that there are discrepancies between tumor cells and craniofacial osteoprogenitors, which need to be further validated.

Here we examined the role of CDC20 specifically in craniofacial MSCs due to site specificity during MSC fate commitment. Mandibular bone marrow-derived MSCs are involved in bone healing (Chung et al., 2009; Lee et al., 2019). Cranial suture-derived MSCs undergo intramembranous growth to expand cranial bone (Li et al., 2021; James et al., 2010). Similar to long bone marrow-derived MSCs, mandibular bone marrow-derived MSCs and cranial suture-derived MSCs can differentiate into osteoblasts and can be used in tissue engineering. However, they differ in their embryonic, phenotypic, and pathological characteristics (Chai et al., 2000; Jiang et al., 2002; Mackie et al., 2008; Aghaloo et al., 2010; Le Douarin and Dupin, 2012; Li et al., 2020). Cranial suture-derived MSCs and mandibular bone marrow-derived MSCs develop from cranial neural crest cells. However, the molecular mechanisms regulating osteogenesis in craniofacial bones differ to those of long bones (Helms and Schneider, 2003). Therefore, it is necessary to elucidate whether CDC20 promotes osteogenesis in craniofacial bones; our findings were consistent with those of a previous study (Du et al., 2021). Nevertheless, the underlying mechanisms remain elusive and should be explored further in subsequent studies.

5. Conclusion

In this study, we demonstrated that conditional knockout of *Cdc20* led to reduced craniofacial bone mass in mice. Osteogenic differentiation in craniofacial bone-derived MSCs was also downregulated. Our results suggest that CDC20 promotes osteogenesis in craniofacial bones, providing a novel target for developing strategies to treat craniofacial bone defects. These findings, which provide insight into the function of CDC20 in craniofacial bone, may advance medical restoration and reconstruction of craniofacial bone defects, providing a promising future for craniofacial bone regeneration.

Ethics approval and consent to participate

All animal procedures and experiments were approved by the Institutional Animal Care and Use Committee of the Peking University Health Science Center (approval number: LA2021006). All procedures of in vivo study on the animals were carried in accordance with the National Institutes of Health guide for the care and use of Laboratory animals and ARRIVE guidelines.

Funding

Consent for publication

Not applicable.

Authors contribution

P.Z., X.Z. and Y.L.: conception and design, financial support, and manuscript writing. Y.D. and Y.C.: laboratory work, collection and analyses of data, manuscript writing. All authors read and approved the final manuscript.

Data Availability

Data sharing not applicable to this article as no datasets were generated or analysed during the current study.

Acknowledgements

Not applicable.

Competing interests

The authors declare that they have no competing interests.

References

Aghaloo, T.L., Chaichanasakul, T., Bezouglaia, O., Kang, B., Franco, R., Dry, S.M., Atti, E., Tetradis, S., 2010. Osteogenic potential of mandibular vs. long-bone marrow stromal cells. J. Dent. Res. 89 (11), 1293–1298.

Atsawasuwan, P., Ouibaidin, M., Dalal, B., Khan, H., Mohammed, A., 2017. Calvarial bone development and suture closure in Dicer-deficient mice. Orthod. Craniofacial Res. 20, 26–31.

Biosse Duplan, M., Dambroise, E., Estibals, V., Veziers, J., Guicheux, J., Legeai-Mallet, L., 2021. An Fgfr3-activating mutation in immature murine osteoblasts affects the appendicular and craniofacial skeleton. Dis. Models Mech. 14 (4) dmm048272.

Cain, C.J., Gaborit, N., Lwin, W., Barruet, E., Ho, S., Bonnard, C., Hamamy, H., Shboul, M., Reversade, B., Kayserili, H., Bruneau, B.G., Hsiao, E.C., 2016. Loss of Iroquois homeobox transcription factors 3 and 5 in osteoblasts disrupts cranial mineralization. Bone Rep. 5, 86–95.

Celil, A.B., Campbell, P.G., 2005. BMP-2 and insulin-like growth factor-I mediate Osterix (Osx) expression in human mesenchymal stem cells via the MAPK and protein kinase D signaling pathways. J. Biol. Chem. 280 (36), 31353–31359.

Chai, Y., Jiang, X., Ito, Y., Bringas P Jr., Jr Han, J., Rowitch, D.H., Soriano, P., McMahon, A.P., Sucov, H.M., 2000. Fate of the mammalian cranial neural crest during tooth and mandibular morphogenesis. Development 127 (8), 1671–1679.

Chang, D.Z., Ma, Y., Ji, B., Liu, Y., Hwu, P., Abbruzzese, J.L., Logsdon, C., Wang, H., 2012. Increased CDC20 expression is associated with pancreatic ductal adenocarcinoma differentiation and progression. J. Hematol. Oncol. 5, 15.

Chen, Y., Fan, Q., Zhang, H., Tao, D., Wang, Y., Yue, R., Sun, Y., 2021. Lineage tracing of cells expressing the ciliary gene IFT140 during bone development. Dev. Dyn. 250 (4), 574–583.

Chung, I.H., Yamaza, T., Zhao, H., Choung, P.H., Shi, S., Chai, Y., 2009. Stem cell property of postmigratory cranial neural crest cells and their utility in alveolar bone regeneration and tooth development. Stem Cells 27 (4), 866–877.

Du, Y., Zhang, M., Liu, X., Li, Z., Hu, M., Tian, Y., Lv, L., Zhang, X., Liu, Y., Zhang, P., Zhou, Y., 2021. CDC20 promotes bone formation via APC/C dependent ubiquitination and degradation of p65. EMBO Rep. 22 (9), e52576.

Fliefel, R., Kühnisch, J., Ehrenfeld, M., Otto, S., 2017. Gene therapy for bone defects in oral and maxillofacial surgery: a systematic review and meta-analysis of animal studies. Stem Cells Dev. 26 (4), 215–230.

Gao, Y., Guo, C., Fu, S., Cheng, Y., Song, C., 2021. Downregulation of CDC20 suppressed cell proliferation, induced apoptosis, triggered cell cycle arrest in osteosarcoma cells, and enhanced chemosensitivity to cisplatin. Neoplasma 68 (2), 382–390.

Harley, M.E., Allan, L.A., Sanderson, H.S., Clarke, P.R., 2010. Phosphorylation of Mcl-1 by CDK1-cyclin B1 initiates its Cdc20-dependent destruction during mitotic arrest. Embo J. 29 (14), 2407–2420.

Helms, J.A., Schneider, R.A., 2003. Cranial skeletal biology. Nature 423 (6937), 326–331.

James, A.W., Xu, Y., Wang, R., Longaker, M.T., 2008. Proliferation, osteogenic differentiation, and fgf-2 modulation of posterofrontal/sagittal suture-derived mesenchymal cells in vitro. Plast. Reconstr. Surg. 122 (1), 53–63.

James, A.W., Levi, B., Commons, G.W., Glotzbach, J., Longaker, M.T., 2010. Paracrine interaction between adipose-derived stromal cells and cranial suture-derived mesenchymal cells. Plast. Reconstr. Surg. 126 (3), 806–821.

Ji, P., Smith, S.M., Wang, Y., Jiang, R., Song, S.W., Li, B., Sawaya, R., Bruner, J.M., Kuang, J., Yu, H., Fuller, G.N., Zhang, W., 2010. Inhibition of gliomagenesis and attenuation of mitotic transition by MIIP. Oncogene 29 (24), 3501–3508.

Jiang, X., Iseki, S., Maxson, R.E., Sucov, H.M., Morriss-Kay, G.M., 2002. Tissue origins and interactions in the mammalian skull vault. Dev. Biol. 241 (1), 106–116.

Kaltschmidt, B., Kaltschmidt, C., Widera, D., 2012. Adult craniofacial stem cells: sources and relation to the neural crest. Stem Cell Rev. Rep. 8 (3), 658–671.

Karra, H., Repo, H., Ahonen, I., Löyttyniemi, E., Pitkänen, R., Lintunen, M., Kuopio, T., Söderström, M., Kronqvist, P., 2014. Cdc20 and securin overexpression predict short-term breast cancer survival. Br. J. Cancer 110 (12), 2905–2913.

Kidokoro, T., Tanikawa, C., Furukawa, Y., Katagiri, T., Nakamura, Y., Matsuda, K., 2008. CDC20, a potential cancer therapeutic target, is negatively regulated by p53. Oncogene 27 (11), 1562–1571.

Lara-Gonzalez, P., Kim, T., Oegema, K., Corbett, K., Desai, A., 2021. A tripartite mechanism catalyzes Mad2-Cdc20 assembly at unattached kinetochores. Science 371 (6524), 64–67.

Le Douarin, N.M., Dupin, E., 2012. The neural crest in vertebrate evolution. Curr. Opin. Genet. Dev. 22 (4), 381–389.

Lee, D.J., Kwon, J., Current, L., Yoon, K., Zalal, R., Hu, X., Xue, P., Ko, C.C., 2019. Osteogenic potential of mesenchymal stem cells from rat mandible to regenerate critical sized calvarial defect. J. Tissue Eng. 10, 2041731419830427, 2041731419830427.

Li, B., Wang, Y., Fan, Y., Ouchi, T., Zhao, Z., Li, L., 2021. Cranial suture mesenchymal stem cells: insights and advances. Biomolecules 11 (8), 1129.

Li, C., Wang, F., Zhang, R., Qiao, P., Liu, H., 2020. Comparison of proliferation and osteogenic differentiation potential of rat mandibular and femoral bone marrow mesenchymal stem cells in vitro. Stem Cells Dev. 29 (11), 728–736.

Liu, J., Liang, C., Guo, B., Wu, X., Li, D., Zhang, Z., Zheng, K., Dang, L., He, X., Lu, C., Peng, S., Pan, X., Zhang, B.T., Lu, A., Zhang, G., 2017. Increased PLEKHO1 within osteoblasts suppresses Smad-dependent BMP signaling to inhibit bone formation during aging. Aging Cell 16 (2), 360–376.

Lloyd, B., Tee, B.C., Headley, C., Emam, H., Mallery, S., Sun, Z., 2017. Similarities and differences between porcine mandibular and limb bone marrow mesenchymal stem cells. Arch. Oral Biol. 77, 1–11.

Mackie, E.J., Ahmed, Y.A., Tatarczuch, L., Chen, K.S., Mirams, M., 2008. Endochondral ossification: how cartilage is converted into bone in the developing skeleton. Int. J. Biochem. Cell Biol. 40 (1), 46–62.

Nakashima, K., Zhou, X., Kunkel, G., Zhang, Z., Deng, J.M., Behringer, R.R., de Crombrugghe, B., 2002. The novel zinc finger-containing transcription factor osterix is required for osteoblast differentiation and bone formation. Cell 108 (1), 17–29.

Percival, C.J., Richtsmeier, J.T., 2013. Angiogenesis and intramembranous osteogenesis. Dev. Dyn. 242 (8), 909–922.

Rodda, S.J., McMahon, A.P., 2006. Distinct roles for Hedgehog and canonical Wnt signaling in specification, differentiation and maintenance of osteoblast progenitors. Development 133 (16), 3231–3244.

Thomas, N., Choi, H.K., Wei, X., Wang, L., Mishina, Y., Guan, J.L., Liu, F., 2019. Autophagy regulates craniofacial bone acquisition. Calcif. Tissue Int. 105 (5), 518–530.

Xu, Y., Malladi, P., Chiou, M., Longaker, M.T., 2007. Isolation and characterization of posterofrontal/sagittal suture mesenchymal cells in vitro. Plast. Reconstr. Surg. 119 (3), 819–829.

Yamaza, T., Ren, G., Akiyama, K., Chen, C., Shi, Y., Shi, S., 2011. Mouse mandible contains distinctive mesenchymal stem cells. J. Dent. Res. 90 (3), 317–324.

Yang, Y., Kim, A.H., Yamada, T., Wu, B., Bilimoria, P.M., Ikeuchi, Y., de la Iglesia, N., Shen, J., Bonni, A., 2009. A Cdc20-APC ubiquitin signaling pathway regulates presynaptic differentiation. Science 326 (5952), 575–578.

Yu, H., 2007. Cdc20: a WD40 activator for a cell cycle degradation machine. Mol. Cell 27 (1), 3–16.

Zhao, H., Chai, Y., 2015. Stem cells in teeth and craniofacial bones. J. Dent. Res 94 (11), 1495–1501.

Zhao, S., Zhang, Y., Lu, X., Ding, H., Han, B., Song, X., Miao, H., Cui, X., Wei, S., Liu, W., Chen, S., Wang, J., 2021. CDC20 regulates the cell proliferation and radiosensitivity of P53 mutant HCC cells through the Bcl-2/Bax pathway. Int. J. Biol. Sci. 17 (13), 3608–3621.

Zhou, S., Li, G., Zhou, T., Zhang, S., Xue, H., Geng, J., Liu, W., Sun, Y., 2021. The role of IFT140 in early bone healing of tooth extraction sockets. Oral Dis. 28, 1188–1197. https://doi.org/10.1111/odi.13833.

Zhou, X., Zhang, Z., Feng, J.Q., Dusevich, V.M., Sinha, K., Zhang, H., Darnay, B.G., de Crombrugghe, B., 2010. Multiple functions of Osterix are required for bone growth and homeostasis in postnatal mice. Proc. Natl. Acad. Sci. USA 107 (29), 12919–12924.